ACS OMEGA

http://pubs.acs.org/journal/acsodf

Article

Fabrication of Hierarchical Patterned Surfaces Using a Functionalized CeO_2-EPDM Composite for Crevice Corrosion Prevention on High-Voltage Insulators

Simpy Sanyal, Taeyong Kim, Ramachandran Chelliah, Deog-Hwan Oh, Duy Phong Pham,* and Junsin Yi*

Cite This: *ACS Omega* 2022, 7, 40920−40928

Read Online

ACCESS | Metrics & More | Article Recommendations

ABSTRACT: Crevice corrosion accounts for 62% of the recorded breakdown of insulators utilized in transmission lines, which may interfere with the reliability of power utilities. To address these challenges, sustainable and resilient slippery lubricant-infused porous surfaces (SLIPS) are developed on insulators to prevent electrochemically/biochemically induced crevice corrosion especially occurring in tropical and coastal environments. The conventional way of developing SLIPS by chemical and physical etching might interfere with the mechanical stability of insulators composed of pin (galvanized steel), cement, and shell (porcelain). The current study proposes a noble concept of developing hierarchical patterned textured surfaces on insulators to fabricate a resilient SLIPS coating without physical/chemical etching. The proposed coating exhibits 99% antiadhesion performance against a mixed culture of bacterial strains, superior hydrophobicity (contact angle: 160°, contact angle hysteresis: 4°), and crevice corrosion resistance performance at elevated temperatures (25−75 °C) and humidity. This study could facilitate a new route for the development of sustainable and highly reliable SLIPS coatings in the future.

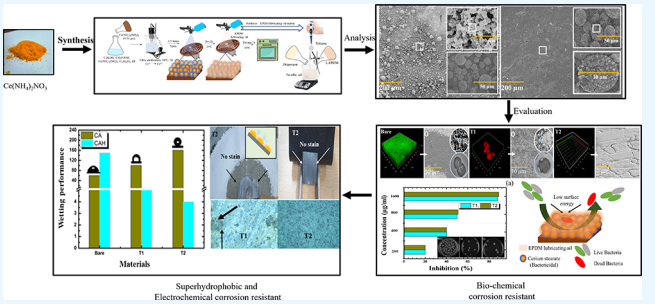

1. INTRODUCTION

The evidence so far suggests that the presence of microbes inside crevices frequently results in highly localized changes in electrolyte constituent concentrations, pH, and oxygen levels.[1−3] The crevice becomes oxygen-depleted, while the surrounding electrolyte gains oxygen, allowing this crevice system to exist. As a result, the material within this crevice system serves as the anode, and the exterior serves as the cathode, completing the redox system. The increase in M^+ ions within the material crevice causes an influx of chloride ions, which results in a net neutralization reaction. The metal chloride is then hydrolyzed to produce a free acid, resulting in an acidic reaction.[4] The hydrolysis reaction produces free acid, which keeps the pH below 2, while the pH outside the crevice remains neutral. Because of the microenvironment and pH state, the electrolyte within the crevice contains a high concentration of metal chloride ions, which are dissolved at near-total saturation concentrations. The biofilm can accelerate oxygen depletion inside the crevice. The respiring microbial colonies within the crevice become anodic, causing the surrounding areas to become cathodic. Two different oxygen concentrations in two different locations result in a difference in electrical potential and, as a result, crevice corrosion.[5,6]

Microorganism development has been evidenced in both ceramic and nonceramic insulators placed all over the world, particularly in tropical and subtropical conditions with high humidity, significant rainfall, and high temperature. It has been found that heterogeneous populations of bacteria, algae, moss, and fungus coexist in insulator biofilms. Single-celled green algae, which is abundant in Asia, is the most commonly discovered biofouling on insulators (Figure 1). The intriguing part about dry algae colonies on insulator surfaces is that they began to develop again when moist.[7−9]

According to published research, the formation of a biofilm layer on the surface of an insulator poses a significant risk of crevice corrosion within an insulator's pin−cement crevice. Crevice corrosion causes crack propagation within the insulator, reduces flashover voltage by 30%, and induces surface leakage current.[10] Such conditions compromise the

Received: June 24, 2022
Accepted: September 2, 2022
Published: November 4, 2022

ACS Publications

© 2022 The Authors. Published by American Chemical Society

https://doi.org/10.1021/acsomega.2c03955
ACS Omega 2022, 7, 40920−40928

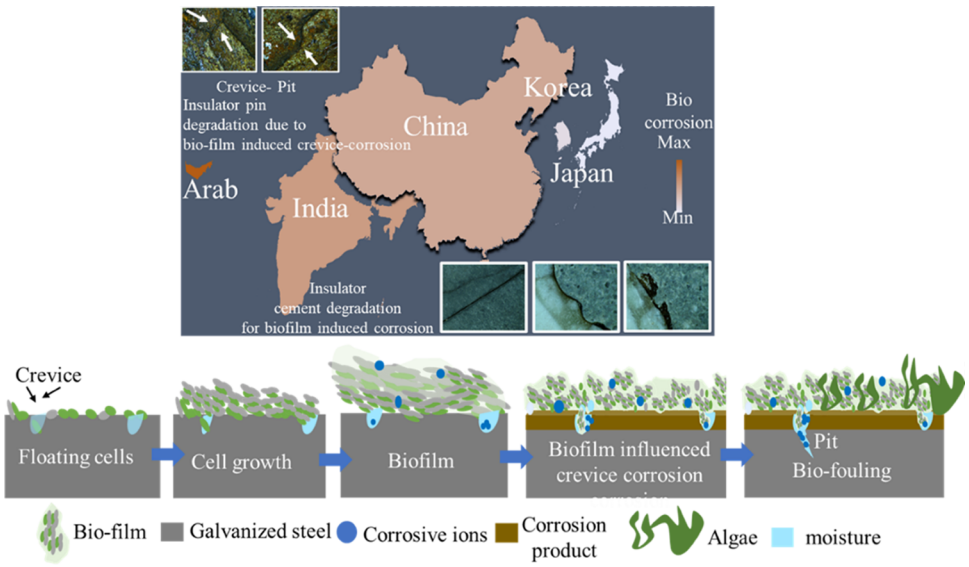

Figure 1. Global implications of biofilm formation on crevice corrosion.

integrity of high-voltage insulators, as shown in Figure 1. Considering the complexity of the situation, it is preferable to limit biofilm formation to avoid abrupt insulator failure.

Most of the available biofilm resistance methods deal with either active coating or passive coating. The first category emits biocides and antibiotics.[10−12] The other category includes antimicrobial chemicals that are securely bound to surfaces, such as hydrophilic polymers and polycationic biocides.[13] The major limitation of the first category is the uncontrolled release of biocides, which decreases over time.[13] Furthermore, both types of coatings promote the formation of an extracellular polymeric adhering film and dead bacteria on coating surfaces, which eventually inhibits initial attachment and has no inhibitory effect over a longer stretch. On the other hand, antimicrobial resistance to the biofilm increases at the same time.[14−16]

Superhydrophobic surfaces have attracted great attention as a green alternative to solve the existing issue.[17] The superhydrophobic surfaces consist of an air layer trapped by micro/nanostructures that prevent direct contact between the corrosive fluid and the surface. The air layer cannot withstand high humidity, air pressure, and biological fluids. Thus, superhydrophobic surfaces cannot be a reliable alternative for the issue.[18]

Over the last decade, surface modification technologies known as slippery liquid-infused porous surfaces (SLIPS) or lubricant-impregnated surfaces (LIS) have evolved. SLIPS coatings have a broad application in marine, biomedical, and construction industries due to their environment-friendly and reliable nature.[19] Until now, several techniques for fabricating SLIPS have been used, including chemical, physical etching, sol−gel synthesis, and so on.[20] However, chemical and physical etching interfere with the mechanical stability of cement and porcelain materials.[21] Similarly, chemical and physical etching are not safe for galvanized steel.[21] Keeping this in mind, a few researchers have used the sol−gel technique to develop SLIPS.[21,22] However, nanopatterns are built on surfaces rather than hierarchical patterns, which have a poorer lubricant retention ability than hierarchical patterns. The stability of SLIPS is based on the capability of surface textures to retain the lubricant by capillary and van der Waals forces.[22] To the best of our knowledge, constructing hierarchical patterned textured surfaces on power insulators without using physical/chemical etching has not been reported so far. In addition, coatings involving cerium are popular as an electrochemical corrosion-resistant material, but its biochemical corrosion resistance has not been explored much.[23]

The current study suggests a noble concept of developing hierarchical patterned textured surfaces on insulators to fabricate a robust SLIPS coating without physical/chemical etching. The efficacy of the proposed treatment has been evaluated systematically against electrochemically and bio-chemically induced crevice corrosion in a simulated tropical and coastal environment.

2. EXPERIMENTAL SECTION

2.1. Materials. The Korea Electric Power Corporation (KEPCO) supplied insulator specimens with a (galvanized steel) pin length of 10.7 cm and a zinc coating of 180 μm. All of the chemicals such as isopropyl alcohol (IPA), Turco 6849, ceric ammonium nitrate $Ce(NH_4)_2NO_3$, ethanol, acetic acid, calcium hydroxide, sodium chloride, and sodium sulfate were procured from Merck, Korea, and liquid ethylene−propylene terpolymers, Trilene 65D (L-EPDM), and dispersant (Disper BYK 2055) were from ChemPoint. All formulations were created with analytical-grade chemicals in distilled water.

2.2. Fabrication of Specimens. For the preparation of cerium sol precursors, 10 g of ceric ammonium nitrate, $Ce(NH_4)_2NO_3$, were dissolved in 10 mL of ethanol, 5 mL of acetic acid, 1 mL of stearic acid, and 5 mL of DI. The obtained sols were initially dark due to the reduction reaction of Ce^{4+} to Ce^{3+} due to the presence of ethanol.[24] The prepared sols were agitated for 1 h under 60 °C. An EPDM-based lubricating oil was prepared by mixing the dispersant (0.10 mL), transparent paraffin oil (100 mL), toluene (4 mL), and L-EPDM (8 mL) blends and agitating at 2000 rpm for 1 h. The Ce-based obtained composite was sprayed (3−5 times) on insulator samples (T1) and dried at room temperature for 3 h. Finally, the EPDM lubricating oil was coated/sprayed on insulator specimens (T2) by a brush/spray and dried for 1 h at 50 °C.[25] The excess EPDM lubricating oil flowed off during the process.

https://doi.org/10.1021/acsomega.2c03955
ACS Omega 2022, 7, 40920−40928

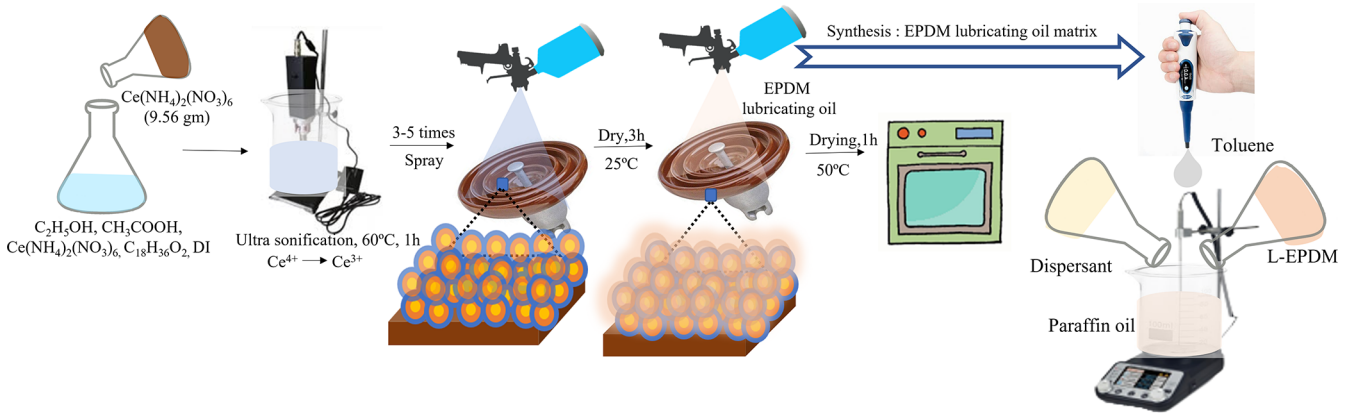

Figure 2. Preparation of the EPDM lubricating oil-infused steric acid-modified cerium oxide composite (hierarchical surface).

The development of composites and application process can be seen in Figure 2.

The dried insulator was cut into 2 cm × 2 cm specimens by waterjet cutting. Three types of specimens were prepared for the experiment: bare (untreated), modified cerium composite-applied specimens (T1), and EPDM lubricating oil-infused steric acid-modified cerium oxide composite-applied specimens (T2). The thicknesses of the coating of T1 and T2 were measured by a laser confocal microscope (36.7 and 37.7 μm, respectively).

2.3. Surface Measurements. The particle size of steric acid-modified cerium oxide can be confirmed with Brookhaven Instruments' dynamic light scattering (DLS) instrument. The morphology and element distribution of the as-prepared specimens was carried out using a scanning electron microscope (SEM, TESCAN, Czech Republic) coupled with energy-dispersive X-ray spectroscopy (EDS). The topology of the as-deposited surfaces was investigated using a Bruker Innova microscope in the high-amplitude mode. Atomic force microscopy (AFM) images were processed using NanoScope analysis 7.0 software to obtain values for roughness characteristics. Fourier transform infrared spectroscopy (FTIR) was carried out by a Bruker IFS-66/S TENSOR 27 instrument with 100 scans and a resolution of 1 cm^{-1}. The water contact angle (WCA) measurements and contact angle hysteresis (CAH) were measured using a Pheonix 300 Touch, and each measurement was repeated three times. The drop volume used was 3 mL. The CAH was calculated as the difference between the advancing and receding contact angles. The variations in WCA and CAH following immersion in corrosive media for 90 days were examined.

2.4. Evaluation of Stability of the Proposed Treatment. The stability of the proposed approach was evaluated by water stress (simulating rain), gravity, and volatility tests. Water drop cloaking tests were set up in a closed flowing water chamber with an inlet and an outlet. The samples (T2) were kept inside the chamber in a horizontal and vertical manner to evaluate stress and gravity tests. The X-ray photoelectron spectroscopy analysis was carried out on the liquid medium filled in the test chamber for five cycles.

For the volatility test, a measured amount of the EPDM lubricating oil (50 mL) was kept in an evaporation crucible and heated to 100 °C for 15 min with a constant flow of air over it. The oil was weighed before and after the test to examine the percent loss in the mass of the oil. The experiment was carried out using the Noack volatility test equipment in accordance with the ASTM D5800 compliant. The result of the experiment was compared with the volatility test results of silicone oil (viscosity: 250 cSt).

2.5. Antiadhesion Tests. *Acidithiobacillus ferroxidans* ATCC 23270 and *Thiobacillus organoparus* Markosian ATCC 27977 bacterial strains were adopted to explore the bacterial antiadhesion of the proposed composite, since this strain forms intense adherent biofilms on various surfaces.

The pin (galvanized steel)/cap (steel)/cement/shell (porcelain) specimens were randomly chosen and incubated in a Petri dish containing mixed cultures of *A. ferroxidans* ATCC 23270 and *T. organoparus* Markosian ATCC 27977 (2×10^{-6} cells/mL) in modified BG11 culture media. The EPDM lubricating oil-infused steric acid-modified cerium oxide composite-applied specimens (T2) were considered. The bare (untreated) and modified Ce composite-treated specimens (T1) were considered reference specimens for the experiment. All samples were rinsed with sterile deionized water and ethanol before culture. The plates containing modified or reference specimens were grown in static circumstances under 2500 lx of white fluorescence light using a 12/12 h light/ dark cycle at room temperature. Each sample comprised three duplicates. After 90 days, the specimens were removed and dried before sending for image analysis.

2.5.1. Antimicrobial Tests. The impact of the modified Ce composite (T1 and T2) on the viability of *A. ferroxidans* ATCC 23270 and *T. organoparus* Markosian ATCC 2797 was examined. The brief twofold dilution of the modified Ce composite and the EPDM lubricating oil-infused steric acid-modified cerium oxide composite with the nutrient broth was carried in triplicate in a 96-well microtiter plate, followed by the addition of 100 μL of combined *A. ferroxidans* ATCC 23270 and *T. organoparus* Markosian ATCC 2797 to each well to provide 13, 7.5, 3.75, 1.89, 0.95, 0.5, 0.2, and 0.1% (v/v) concentration by volume with a final volume of 200 μL. The plate was sealed and incubated at 37 °C. After 1, 6, and 24 h of incubation, 35 μL of each well suspension was removed and cultivated on nutrient agar by the pour plate method. The plate counting (CFU/mL) was performed post incubation at 37 °C.

2.6. Anticorrosion Performance. The anticorrosion performance of bare, modified Ce (T1), and EPDM lubricating oil-infused steric acid-modified cerium oxide composite (T2)-applied specimens were studied in corrosion media for 90 days by a Korean Scientific Inc. UCMOS03100KPA. In addition, electrochemical workstation tests were conducted by measur-

https://doi.org/10.1021/acsomega.2c03955
ACS Omega 2022, 7, 40920−40928

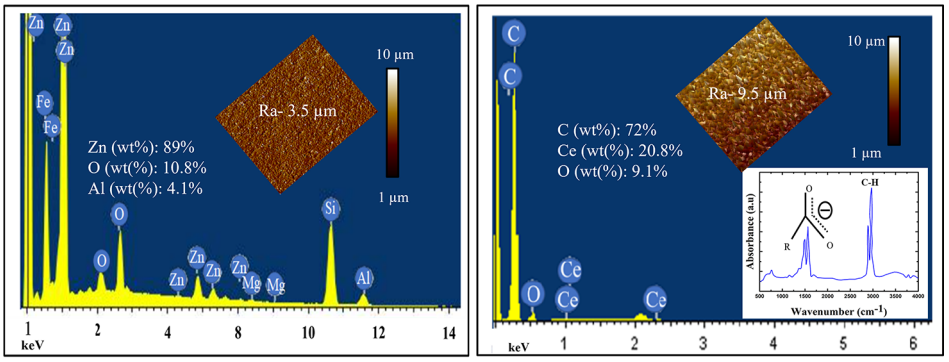

Figure 3. Surface analysis of (a) untreated (bare) and (b) treated specimens (T2).

ing Tafel curves by sweeping the potential from −0.6 to 0.6 V versus the open circuit potential at a rate of 1 mV/s. Electrochemical impedance spectroscopy was determined by altering the frequency range between 10^{-2} and 10^{5} Hz, and the open circuit potential was kept at equilibrium.[24] The corrosion media was prepared by adding 24.12 g NaCl, 4.01 g Na_2SO_4, 5.02 g $MgCl_2$, 1.20 g $CaCl_2$, 0.7 g KCl, 0.20 g $NaHCO_3$, 0.10 g KBr, 0.03 g H_3BO_3, 0.3 g $SrCl_2$, and 0.02 g NaF in 1 L of deionized water.

3. RESULTS AND DISCUSSION

3.1. Surface Morphology and Composition. EDS was used to analyze the surface chemistry of the treated specimens. The contents of unprocessed specimens (bare) were Zn (wt %): 89, O (wt %): 10.8, and Al (wt %): 4.1, with a roughness (R_a) of 3.5 μm, as shown in Figure 3a. In addition, treated specimens (T2) show C (wt %): 72, Ce (wt %): 20.8, and O (wt %): 9.1, with a roughness (R_a) of 9.5 μm, as shown in Figure 3b.

The EDS results suggest that the EPDM lubricating oil-infused steric acid-modified cerium oxide composite was adsorbed on the surface. In the FTIR spectra of the deposited specimens (Figure 3b), peaks 2848 and 2920 cm^{-1} are attributed to the adsorption of C−H asymmetric and symmetric stretching vibrations, revealing the presence of EPDM. The carboxylate peaks are detected at 1448 and 1546 cm^{-1}, reconfirming the adsorption of cerium stearate on the surface.[26]

Stearic acid, $CH_3(CH_2)_{16}COOH$, is ionized to produce $CH_3(CH_2)_{16}COO^-$ ions and H^+ ions in the presence of a catalyst. The $CH_3(CH_2)_{16}COO^-$ ions reside in the cathode region. However, H^+ ions combine with electrons to produce H_2. The Ce^{3+} ions are oxidized to Ce^{4+} ions. With the progress of the reaction, Ce^{4+}, Ce^{3+}, and $CH_3(CH_2)_{16}COO^-$ react and adsorb on the treated specimens (cathode). Cerium stearate is adsorbed on the surface to form microstructures; meanwhile, emitting H_2 facilitates the formation of micro/nanostructures.[26] Thus, the roughness (R_a) of the treated specimen changes to 9.5 μm, as shown in Figure 3b. The chemical processes can be explained using Figure 4.

The particle size of Ce(III) stearate and Ce(IV) stearate was measured to be 10 μm on average by a particle analyzer.

3.2. Surface Wettability. The wettability of the surface is influenced by factors like surface morphology and surface topology. To operate effectively in harsh tropical or coastal environments, the treated insulator should be water repellent,

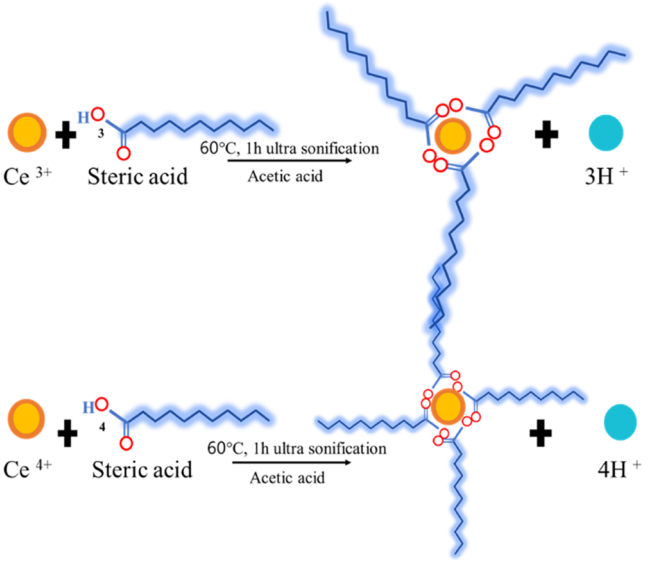

Figure 4. Chemical reaction between Ce ions and stearic acid.

as water infiltration in insulator microcracks is primarily responsible for crevice corrosion and other corrosion. The hydrophobic performances of untreated (bare) and treated specimens (T1 and T2) are compared in Figure 5a. The untreated specimens depict a contact angle (CA) of 60° and a contact angle hysteresis (CAH) of 150°. After treatment, specimen T1 depicts a CA of 150° and a CAH of 10°.

At the same time, specimen T2 depicts a CA of 160° and a CAH of 4°. T1 specimens comprise higher CA due to higher surface roughness, a lower actual contact area, and a long carbon chain of stearic acid adsorbed on globular cerium stearate that supports nanosheet formation (hierarchical structure; Figure 5b). However, due to higher CAH, the water droplets could not slide off the treated substrate, as shown in Figure 6a.

T2 specimens show higher CA and CAH due to the presence of the EPDM-based lubricant oil as a top layer in addition to the hierarchical structure (Figure 5b). The nanosheets on the surface of microspheres and in the gaps between them can provide enough capillary force to retain the EPDM lubricating oil. Due to the presence of the lubricant, the water droplet rolls off the substrates, as shown in Figure 6b. The CA and CAH measurements were carried out on both untreated and treated substrates cut from the insulator, such as pins (galvanized steel) and cement specimens, as shown in

https://doi.org/10.1021/acsomega.2c03955
ACS Omega 2022, 7, 40920−40928

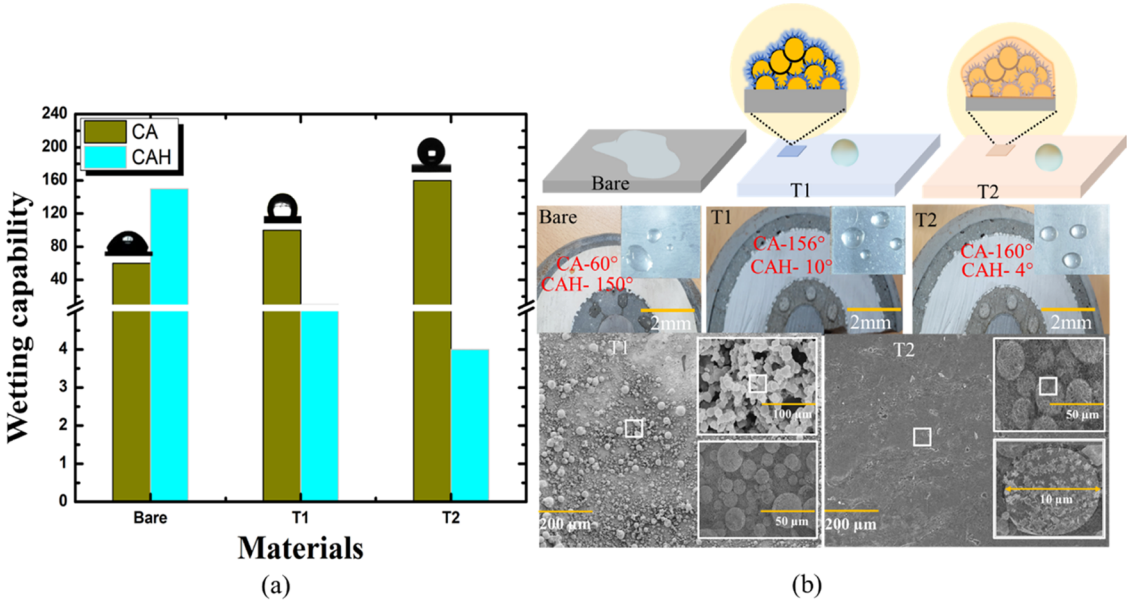

Figure 5. Wettability performance of (galvanized steel and cement) specimens. (a) Contact angle measurements at the planer surface. (b) Water-repelling performance of water droplets on bare and treated specimens; schematic of the water−surface interface of the bare and treated specimens and the corresponding surface morphology.

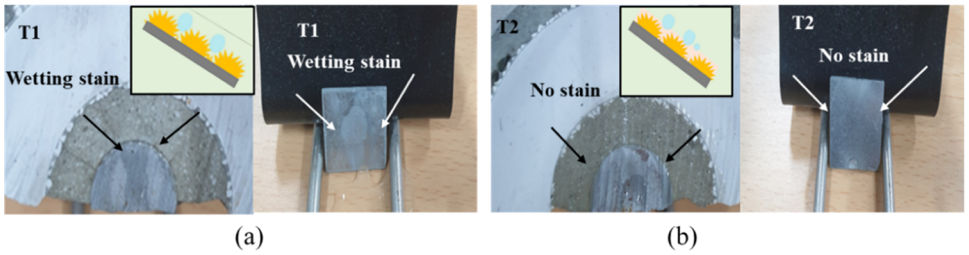

Figure 6. Sliding performance of water droplets on treated specimens at the sliding position: (a) T1 and (b) T2.

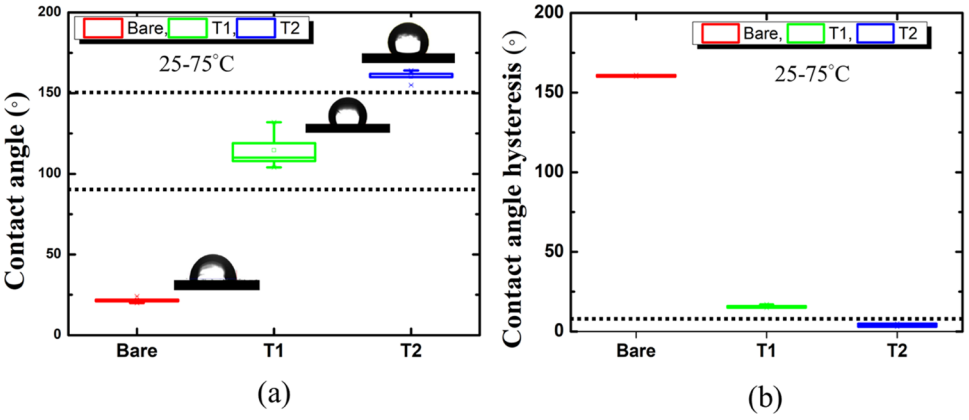

Figure 7. Wettability performance after exposure to corrosive media with varying temperatures from 25 to 75 °C: (a) contact angle measurements and (b) contact angle hysteresis measurements.

Figures 5b and6a,b. In addition, contact of bare and treated specimens (T1 and T2) with water and corresponding micrographs revealing the morphology of treated specimens are depicted in Figures 5b and 6a,b.

For the evaluation of the stability of treated specimens in harsh conditions, the hydrophobic performance was re-examined after exposure to corrosion media for 90 days at a temperature range of 25−75 °C (see Figure 7). The CA of specimen T1 reduces to 115° and its CAH increases to 16°. The reason could be the solubility of stearate-based nanosheets under harsh conditions.[27] However, T2 specimens have shown stable CA and CAH under harsh conditions. The probable explanation could be that due to lower CAH, the corrosive solution droplets could easily roll off the substrate. The liquid repellency attitude of T2 specimens under any condition is attributed to the EPDM lubricating oil on the top layer. If the substrate has crevices/microcracks, the lubricant will penetrate the crevice and prevent the entry of liquid/corrosive liquid,

https://doi.org/10.1021/acsomega.2c03955
ACS Omega 2022, 7, 40920−40928

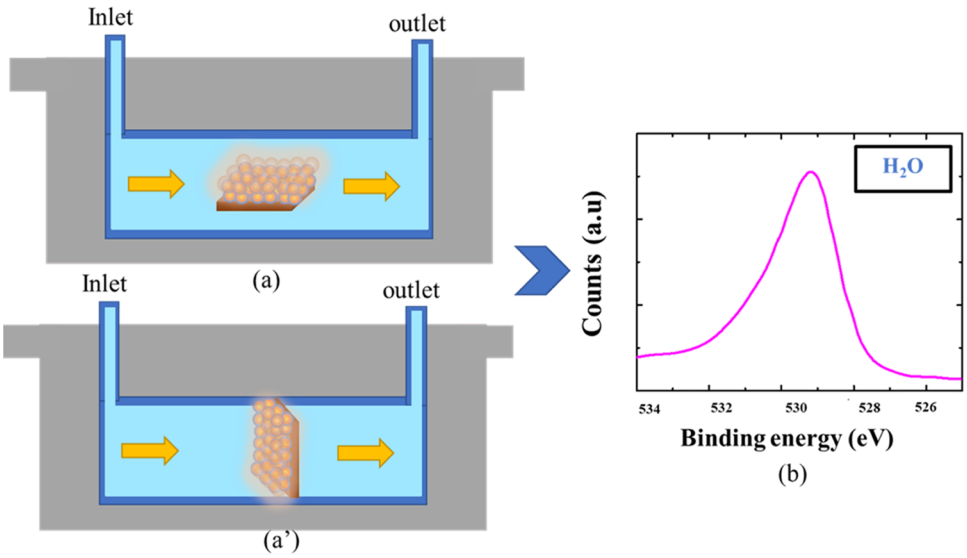

Figure 8. Experimental setup to examine the stability of T2 (a,a′). In flowing water/rain at horizontal and vertical positions. (b) XPS of liquid media coming out from the outlet of the setup (a,b).

which is the source of crevice corrosion. This excellent performance has made the treatment (T2) ideal for usage in extreme conditions, including higher temperatures up to 75 °C.[28] Additionally, the aged samples T2 underwent five cycles of simulating rainstorms to test their lubricant resilience against stress and gravity. Figure 8a,a′ depicts the experimental setup. The flowing water (five cycles) from the setup's output was subjected to XPS (Figure 8b), but no evidence of the EPDM lubricating oil was discovered. The stability of the lubricating oil was further reconfirmed by the Noack volatility test. Only 7% of the EPDM lubricating oil was lost when heated over >75−100 °C for 15 min (see Figure 9). The results are in line with silicone oil (200 cSt). Thus, it is confirmed that the proposed approach for SLIPS fabrication is stable.

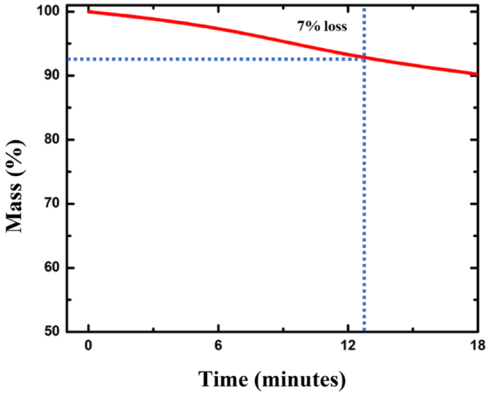

Figure 9. Volatility results for the lubricating EPDM oil.

3.3. Antibiofilm Performance. The accumulation of bacteria, diatoms, and other microorganisms on the surface of the insulator is primarily responsible for biofilm development. Since a biofilm may change the microenvironment of crevices, it causes significant crevice corrosion. Reduced biofilm development can considerably reduce the massive damage caused by the future establishment of crevice corrosion, biocorrosion, and macrofouling biological populations. For biofilm antiadhesion testing, a mixed culture of *A. ferroxidans* ATCC 23270 and *T. organoparus* Markosian ATCC 27977 bacterial strains was chosen. The three substrates bare, T1, and T2 were kept in the bacterial suspension for 90 days and studied, as shown in Figure 10. The bare substrate was covered with a dense layer of living cells (green), resulting in biofilm development, as illustrated in Figure 10a by confocal and corresponding SEM micrographs. The treated specimens (T1 and T2) showed antiadhesive performance against the bacterial population.

The confocal and SEM micrographs of the treated substrate (T1) show minimal bacterial adherence and simultaneous fatal effect (red) on the attached bacterial population. The corresponding SEM micrographs demonstrate bacterial cell wall breakdown of the attached bacterial population. The reason might be the fewer attachment points of the hierarchal structure formed on specimen T1 and the bactericidal effect of Ce (see Figure 10a).[29] For specimen T2, the confocal micrograph depicts no bacterial adhesion. The reason might be that even if a small number of bacteria clings to the substrate and die, the dead bacterial population does not bind to the substrate for an extended period due to the extremely low surface energy of the top EPDM lubricating oil, and the result is reconfirmed by the corresponding SEM micrograph (see Figure 10a). The fatal effect of Ce(III) stearate and the EPDM lubricating oil-infused Ce(III) stearate composite was reconfirmed by the CFU/mL test, as shown in Figure 10b. The schematic of the antibiofilm and bactericidal efficacy of composite T2 is represented in Figure 10c. The statistical analysis reveals that the adhesion ratios for bare and treated substrates (T1 and T2) were 63.3, 3.8, and 0.1% respectively. The proposed treatment (T2) illustrates dual protection from the microbial population by prevention of adherence (99%) and fatal effect (0.1%). The removal of the dead bacterial population attached to the proposed treatment (T2) due to extremely low surface energy is an added advantage.

3.4. Anticorrosion Performance. The anticorrosion performance is an essential assessment for coatings applied to insulators installed in tropical and coastal regions. To evaluate the corrosion performance of the proposed treatment,

https://doi.org/10.1021/acsomega.2c03955
ACS Omega 2022, 7, 40920−40928

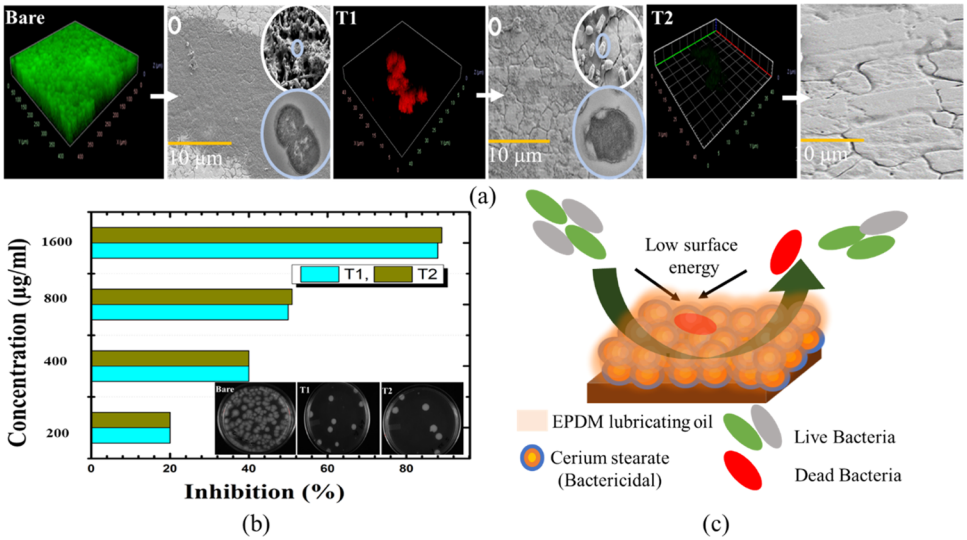

Figure 10. Biofilm resistance performance of treatment: (a) antiadhesion performance, (b) fatal effect, and (c) schematic of the biofilm resistance efficacy of T2.

the bare and treated substrates (T1 and T2) are studied after exposure to corrosion media for 90 days at 25−75 °C, as shown in Figure 11a−c. The untreated crevice can quickly develop localized corrosion in the presence of corrosive fluids, leading to crevice or pitting corrosion. The topology of the crevice formed in metal−nonmetal joints is most susceptible to local corrosion under harsh microenvironments.[30−32] Thus, the crevice of pin (galvanized steel)−cement was studied to evaluate the progress of any local corrosion in the bare and treated substrates. The crevice found in the untreated and T1 treated pin−cement joint reveals symptoms of corrosion in pin (galvanized steel) and cement deterioration, as exhibited in Figure 11a,b. The early indications of deterioration in the pin−cement junction found in T1 treated specimens may be caused due to solubility of cerium stearate under very harsh conditions. However, the excellent corrosion performance of the T2 treated specimen is related to stable lubricating oil (EPDM oil) and the hierarchical structure that serves as a barrier against penetration of corrosive fluids inside the crevice.

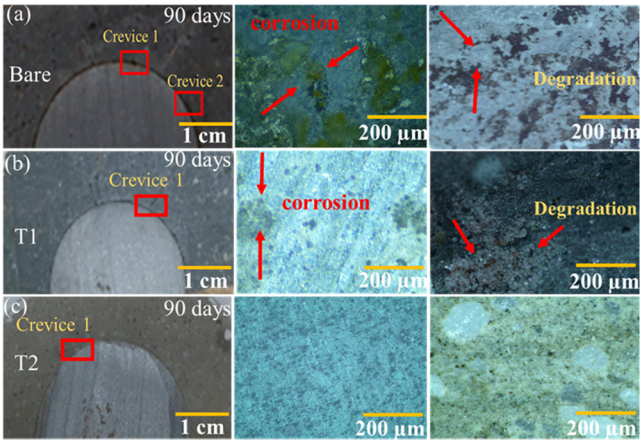

Figure 11. Anticorrosion performance of bare and treated pin (galvanized steel)−cement joint specimens after exposure to corrosion media for 90 days at 25−75 °C: (a) bare, (b) T1, and (c) T2.

Additionally, potentiodynamic polarization and electrochemical impedance spectroscopic studies were performed to reconfirm the corrosion resistance properties of the treated specimens (see Figure 12).

The corrosion current density, I_{corr}, and the corrosion rate (CR) for the bare specimen are highest (4.61×10^{-6} A/cm^2 and 5.41×10^{-2} mm/Y, respectively) over the treated specimens (T1 and T2). However, T2 has I_{corr} and CR 1 order of magnitude lesser than T1 (see Figure 12a). The Bode and Nyquist plots represent the highest capacitance for T2, which is also in line with the previous findings (see Figure 12b−d). Therefore, the proposed composite T2 exhibit the best corrosion resistance against biochemical and electrochemical corrosion.

4. CONCLUSIONS

The study introduced a strategy to develop lubricating oil-infused hierarchical patterned porous surfaces on insulators by utilizing the EPDM lubricating oil-infused steric acid-modified cerium oxide composite (green composite) to prevent electrochemically/biochemically induced crevice corrosion in the tropical and coastal environment. The surface analysis results utilizing EDS, FTIR, and AFM suggested the existence of EPDM lubricating oil-infused cerium stearate on the surface. The superhydrophobic property (CA of 160° and CAH of 4°) of the proposed composite (T2) before and after exposure to corrosion media at 25−75 °C was validated by contact angle measurements and macrographs. The schematic and the corresponding SEM micrographs revealed the superhydrophobic performance of the lubricant-infused hierarchical surface developed on treated substrate T2. This excellent water-repelling performance and acquired stability have made the treatment (T2) ideal for usage in extreme conditions, including tropical and coastal regions. The confocal and SEM images confirm the efficacy of the proposed treatment (T2) against the microbial population by preventing adherence (99%) and fatal effects (0.1%). The removal of the dead bacterial population attached to the surface due to extremely low surface energy is an added advantage. The antielectrochemical corrosion property of the proposed composite was validated by image analysis, potentiodynamic polarization, and electro-

https://doi.org/10.1021/acsomega.2c03955
ACS Omega 2022, 7, 40920−40928

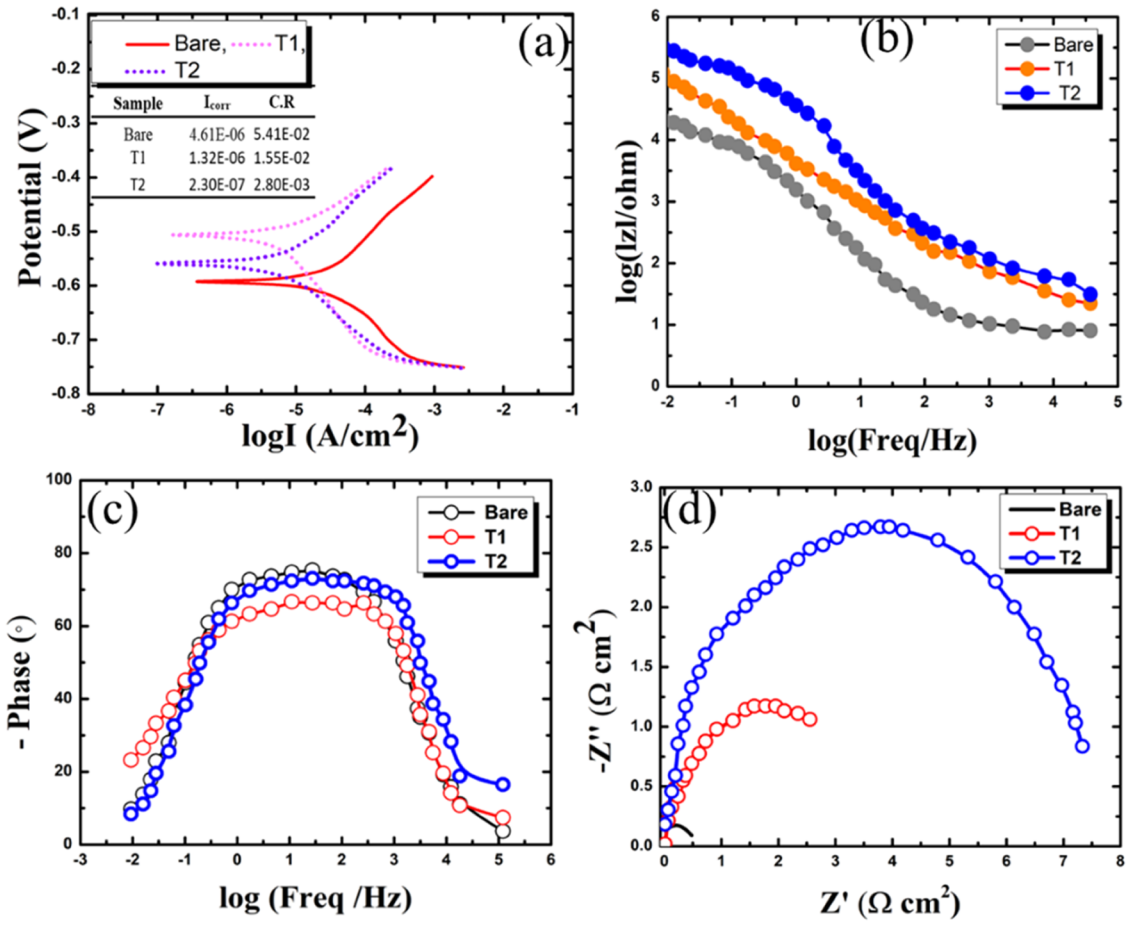

Figure 12. (a) Tafel polarization curves. Electrochemical impedance spectroscopic studies: (b) Bode magnitude plots, (c) Bode phase plots, and (d) Nyquist plots.

chemical impedance spectroscopic studies. Thus, the proposed treatment is an encouraging green solution against electro-chemical- and biochemical-inspired crevice corrosion of insulators installed in tropical and coastal regions and leads to the safe operation of power utilities.

AUTHOR INFORMATION

Corresponding Authors

Duy Phong Pham − *Department of Electrical and Computer Engineering, Sungkyunkwan University, Suwon 16419, Republic of Korea;* orcid.org/0000-0002-0512-4665; Email: pdphong@skku.edu

Junsin Yi − *College of Information and Communication Engineering, Sungkyunkwan University, Suwon 16419, Republic of Korea*; Email: junsin@skku.edu

Authors

Simpy Sanyal − *Department of Electrical and Computer Engineering, Sungkyunkwan University, Suwon 16419, Republic of Korea*

Taeyong Kim − *Department of Electrical and Computer Engineering, Sungkyunkwan University, Suwon 16419, Republic of Korea*

Ramachandran Chelliah − *Department of Food Science and Biotechnology, College of Agriculture and Life Sciences, Kangwon National University, Chuncheon 24341, Republic of Korea; Kangwon Institute of Inclusive Technology (KIIT), Kangwon National University, Chuncheon 24341, Korea; Saveetha School of Engineering, (SIMATS) University, Tamil Nadu 600124, India*

Deog-Hwan Oh − *Department of Food Science and Biotechnology, College of Agriculture and Life Sciences, Kangwon National University, Chuncheon 24341, Republic of Korea*

Complete contact information is available at: https://pubs.acs.org/10.1021/acsomega.2c03955

Funding

This research was supported by grants from the New & Renewable Energy Technology Development Program of the Korea Institute of Energy Technology Evaluation and Planning (KETEP) funded by the Korean Ministry of Trade, Industry and Energy (MOTIE), 20224000000360, 20203030010060.

Notes

The authors declare no competing financial interest.

ACKNOWLEDGMENTS

The authors would like to thank Hyun-Ah Lee at the Central Laboratory of the Kangwon National University for instruction and technical support with an SR-CLSM.

REFERENCES

(1) Jafarzadeh, S.; Zhao, J.; Shakouri, M.; Bobaru, F. A Peridynamic Model for Crevice Corrosion Damage. *Electrochim. Acta* **2022**, *401*, No. 139512.

https://doi.org/10.1021/acsomega.2c03955
ACS Omega 2022, 7, 40920−40928

(2) Rabelo, M.; Sanyal, S.; Kim, T.; Son, J. A.; Choi, I. H.; Yi, J. Influence of Electrolytic and Crevice Corrosion on Mechanical Resistance of Porcelain Insulators. *Eng. Failure Anal.* **2021**, *124*, No. 105317.
(3) Chugh, B.; Sheetal; Singh, M.; Thakur, S.; Pani, B.; Singh, A. K.; Saji, V. S. Extracellular Electron Transfer by *Pseudomonas aeruginosa* in Biocorrosion: A Review. *ACS Biomater. Sci. Eng.* **2022**, *8*, 1049−1059.
(4) Ogunsona, E. O.; Muthuraj, R.; Ojogbo, E.; Valerio, O.; Mekonnen, T. H. Engineered Nanomaterials for Antimicrobial Applications: A Review. *Appl. Mater. Today* **2020**, *18*, No. 100473.
(5) Zhao, Q.; Kang, S.; Zou, F.; Zhu, Z.; Kang, J.; Yin, Y. Properties and Corrosion Resistance Mechanism of a Self-Healing Propane − 1, 2, 3-Triol-Loaded Polysulfone Microcapsule Coating Loaded with Epoxy Resin. *ACS Omega* **2022**, *7*, 21868−21876.
(6) Siddiquie, R. Y.; Gaddam, A.; Agrawal, A.; Dimov, S. S.; Joshi, S. S. Anti-Biofouling Properties of Femtosecond Laser-Induced Sub-micron Topographies on Elastomeric Surfaces. *Langmuir* **2020**, *36*, 5349−5358.
(7) Sotoodeh, K.; Karim, M. F.; Hamdi, Z.; Karthick, S.; Muralidharan, S.; Saraswathy, V.; Chauhan, D. S.; Verma, C.; Quraishi, M. A.; Deng, R.; Shen, T.; Chen, H.; Lu, J.; Yang, H. C.; Li, W. A Review and Analysis of Industrial Valve Material Failures Due to Corrosion and Proposals for Prevention Measures Based on Industrial Experiences in the Offshore Sector of the Oil and Gas Industry. *Arab. J. Chem.* **2020**, *1227*, 3301−3318.
(8) Ferreira, O.; Rijo, P.; Gomes, J. F.; Santos, R.; Monteiro, S.; Vilas-Boas, C.; Correia-Da-Silva, M.; Almada, S.; Alves, L. G.; Bordado, J. C.; Silva, E. R. Biofouling Inhibition with Grafted Econea Biocide: Toward a Nonreleasing Eco-Friendly Multiresistant Anti-fouling Coating. *ACS Sustainable Chem. Eng.* **2020**, *8*, 12−17.
(9) Kumara, S.; Fernando, M. Performance of Outdoor Insulators in Tropical Conditions of Sri Lanka. *IEEE Electr. Insul. Mag.* **2020**, *36*, 26−35.
(10) Hölzl, G.; Luckeneder, G.; Duchaczek, H.; Kleber, C.; Hassel, A. W. Evolution and Interaction of Corrosive Species during the Initial NaCl Particle Induced Corrosion on Zinc Coated Skin-Passed Steel. *Corros. Sci.* **2017**, *127*, 222−229.
(11) Song, F.; Zhang, L.; Chen, R.; Liu, Q.; Liu, J.; Yu, J.; Liu, P.; Duan, J.; Wang, J. Bioinspired Durable Antibacterial and Antifouling Coatings Based on Borneol Fluorinated Polymers: Demonstrating Direct Evidence of Antiadhesion. *ACS Appl. Mater. Interfaces* **2021**, *13*, 33417−33426.
(12) Kung, M. L.; Lin, P. Y.; Peng, S. W.; Wu, D. C.; Wu, W. J.; Yeh, B. W.; Tai, M. H.; Hung, H. S.; Hsieh, S. Biomimetic Polymer-Based Ag Nanocomposites as a Antimicrobial Platform. *Appl. Mater. Today* **2016**, *4*, 31−39.
(13) Akhavan, B.; Michl, T. D.; Giles, C.; Ho, K.; Martin, L.; Sharifahmadian, O.; Wise, S. G.; Coad, B. R.; Kumar, N.; Griesser, H. J.; Bilek, M. M. Plasma Activated Coatings with Dual Action against Fungi and Bacteria. *Appl. Mater. Today* **2018**, *12*, 72−84.
(14) Mendhi, J.; Asgari, M.; Ratheesh, G.; Prasadam, I.; Yang, Y.; Xiao, Y. Dose Controlled Nitric Oxide-Based Strategies for Antibacterial Property in Biomedical Devices. *Appl. Mater. Today* **2020**, *19*, No. 100562.
(15) Suganya Bharathi, B.; Stalin, T. Cerium Oxide and Peppermint Oil Loaded Polyethylene Oxide/Graphene Oxide Electrospun Nanofibrous Mats as Antibacterial Wound Dressings. *Mater. Today Commun.* **2019**, *21*, No. 100664.
(16) Han, G.; Nguyen, T. B.; Park, S.; Jung, Y.; Lee, J.; Lim, H. Moth-Eye Mimicking Solid Slippery Glass Surface with Icephobicity, Transparency, and Self-Healing. *ACS Nano* **2020**, *14*, 10198−10209.
(17) Hwang, G. B.; Page, K.; Patir, A.; Nair, S. P.; Allan, E.; Parkin, I. P. The Anti-Biofouling Properties of Superhydrophobic Surfaces Are Short-Lived. *ACS Nano* **2018**, *12*, 6050−6058.
(18) Kim, H. N.; Lee, S. J. Shear-Driven Drainage of Lubricant in a Spherical Cavity of Lubricant-Infused Surface. *Phys. Fluids* **2021**, *33*, No. 122011.
(19) Olad, A.; Maryami, F.; Mirmohseni, A.; Shayegani-Akmal, A. A. Potential of Slippery Liquid Infused Porous Surface Coatings as Flashover Inhibitors on Porcelain Insulators in Icing, Contaminated, and Harsh Environments. *Prog. Org. Coat.* **2021**, *151*, No. 106082.
(20) Noronha, V. T.; Jackson, J. C.; Camargos, C. H. M.; Paula, A. J.; Rezende, C. A.; Faria, A. F. "Attacking-Attacking" Anti-Biofouling Strategy Enabled by Cellulose Nanocrystals-Silver Materials. *ACS Appl. Bio Mater.* **2022**, *5*, 1025−1037.
(21) Yang, C.; He, G.; Zhang, A.; Wu, Q.; Zhou, L.; Hang, T.; Liu, D.; Xiao, S.; Chen, H. J.; Liu, F.; Li, L.; Wang, J.; Xie, X. Injectable Slippery Lubricant-Coated Spiky Microparticles with Persistent and Exceptional Biofouling-Resistance. *ACS Cent. Sci.* **2019**, *5*, 250−258.
(22) Sanyal, S.; Kim, T.; Rabelo, M.; Pham, D. P.; Yi, J. Novel Synthesis of a Self-Healing Ce Based Eco-Friendly Sealing Coating to Mitigate Corrosion in Insulators Installed in Industrial Regions. *RSC Adv.* **2022**, *12*, 2612−2621.
(23) Thiruvoth, D. D.; Ananthkumar, M. Evaluation of Cerium Oxide Nanoparticle Coating as Corrosion Inhibitor for Mild Steel. *Mater. Today: Proc.* **2022**, *49*, 2007−2012.
(24) Sanyal, S.; Kim, T.; Rabelo, M.; Pham, D. P.; Yi, J. Application of Noble Cerium- Based Anti-Corrosion Sealing Coating Approach Applied on Electrical Insulators Installed in Industrial Regions. *R. Soc. Open Sci.* **2022**, *9*, No. 211786.
(25) Wang, N.; Xiong, D.; Lu, Y.; Pan, S.; Wang, K.; Deng, Y.; Shi, Y. Design and Fabrication of the Lyophobic Slippery Surface and Its Application in Anti-Icing. *J. Phys. Chem. C* **2016**, *120*, 11054−11059.
(26) Kumari, S.; Saini, A.; Dhayal, V. Metal Oxide Based Epoxy Coatings for Corrosion Protection of Steel. *Mater. Today: Proc.* **2021**, *43*, 3105−3109.
(27) Zhuo, Y.; Wang, F.; Xiao, S.; He, J.; Zhang, Z. One-Step Fabrication of Bioinspired Lubricant-Regenerable Icephobic Slippery Liquid-Infused Porous Surfaces. *ACS Omega* **2018**, *3*, 10139−10144.
(28) Ahmed, A. H.; Sherif, E.-S. M. Methylenedisalicylic Acid as a Biocorrosion Inhibitor for Aluminum in Concentrated Sodium Chloride Solutions. *ACS Omega* **2022**, *7*, 19193−19203.
(29) Deng, R.; Shen, T.; Chen, H.; Lu, J.; Yang, H. C.; Li, W. Slippery Liquid-Infused Porous Surfaces (SLIPSs): A Perfect Solution to Both Marine Fouling and Corrosion? *J. Mater. Chem. A* **2020**, *8*, 7536−7547.
(30) Mishra, S. R.; Ahmaruzzaman, M. Cerium Oxide and Its Nanocomposites: Structure, Synthesis, and Wastewater Treatment Applications. *Mater. Today Commun.* **2021**, *28*, No. 102562.
(31) Huang, C.; Guo, Z. Fabrications and Applications of Slippery Liquid-Infused Porous Surfaces Inspired from Nature: A Review. *J. Bionic Eng.* **2019**, *16*, 769−793.
(32) Chen, X.; Wen, G.; Guo, Z. What are the design principles, from the choice of lubricants and structures to the preparation method, for a stable slippery lubricant infused porous surface. *Mater. Horiz.* **2020**, *7*, 1697−1726.

https://doi.org/10.1021/acsomega.2c03955
ACS Omega 2022, 7, 40920−40928